

## RESEARCH ARTICLE OPEN ACCESS

# Record-Wise Disaggregated Seismic Fragilities for Interconnected Systems

Nikolaos D. Karaferis<sup>1</sup>  | Vasileios E. Melissianos<sup>1</sup>  | Athanasia K. Kazantzi<sup>2</sup>  | Konstantinos Bakalis<sup>1</sup>  |  
Dimitrios Vamvatsikos<sup>1</sup> 

<sup>1</sup>School of Civil Engineering, National Technical University of Athens, Athens, Greece | <sup>2</sup>Department of Civil Engineering, International Hellenic University, Serres, Greece

**Correspondence:** Nikolaos D. Karaferis ([nkaraferis@mail.ntua.gr](mailto:nkaraferis@mail.ntua.gr))

**Received:** 21 May 2025 | **Revised:** 16 September 2025 | **Accepted:** 30 November 2025

**Keywords:** critical infrastructure | disaggregated fragilities | earthquake | interconnected systems

## ABSTRACT

Seismic risk assessment studies typically rely on fragility functions/curves to characterize the susceptibility of an asset or a class of assets to damage. These curves are essentially a summarization of responses evaluated on the basis of ground motions with record characteristics and intensities that may or may not be tied to a specific site and its hazard. As is typical with intermediate aggregations in a lengthy analysis chain, this operation achieves ease of use by condensing the behavior of each asset into one or more fragilities, at the cost of losing non-negligible information. Specifically, the within-event correlation in response among different assets is removed, eliminating the potential to distinguish a benign from an aggressive event. Whereas this may not be important for assessing damage and loss for a single asset or an ensemble of independent ones, it can become highly influential for an interconnected system of assets, such as critical energy infrastructure, and for compound (concomitant or cascading) hazards. Instead, disaggregating the fragility back into individual ground motion records and separately propagating the consequences to the overall system improves fidelity at the cost of complexity. To investigate the effect of conventional versus disaggregated fragilities, different simplified system topologies are employed, demonstrating cases where the loss of response correlation can lead to severe bias in the impact assessment at the system level.

## 1 | Introduction

Every time we summarize results in a long chain of analyses, we gain in simplicity, but we lose in resolution. Whether this loss is important or can safely be disregarded, is both case- and application-specific. For the probabilistic calculations and Monte Carlo simulations that characterize any seismic risk assessment task, the effect of the summation process on the final outcome remains to be investigated. Consider, for instance, a portfolio of spatially distributed assets. The classic approach is to tackle this portfolio on an asset-by-asset basis and aggregate the losses, essentially using—the nowadays well established—probabilistic seismic hazard assessment (PSHA [1]) products (e.g.,

hazard curves), together with either asset-specific or class-generic fragilities. In other words, both hazard and fragility/vulnerability tend to be employed in their aggregated form, that is, in the form of hazard and fragility/vulnerability curves, respectively. Is this approach valid, or is it prone to bias? For such questions in earthquake engineering, the only definitive answer is “it depends.”

In simple terms and in the context of our discussion, intra-event (within-event) correlation implies the expected “similarity” in ground motion, response, and damage that nearby identical assets will experience when subjected to a given event. This is in addition to the inter-event (event-to-event) correlation,

This is an open access article under the terms of the [Creative Commons Attribution-NonCommercial-NoDerivs](https://creativecommons.org/licenses/by-nc-nd/4.0/) License, which permits use and distribution in any medium, provided the original work is properly cited, the use is non-commercial and no modifications or adaptations are made.

© 2025 The Author(s). *Earthquake Engineering & Structural Dynamics* published by John Wiley & Sons Ltd.

which addresses the fact that events of similar seismological characteristics will also be expected to generate similar ground motion, response, and damage in said assets. To a large extent, inter-event correlation is accounted for by the internal consistency in the seismic source, exposure, and fragility/vulnerability models, as these do not change from event to event. Intra-event correlation, though, is typically disregarded in the classic approach to loss assessment. Therefore, the latter will begin losing in fidelity in cases that the assets (i) are close enough to be affected by a single event, (ii) are interconnected and failure of one can have operational or even physical consequences on the others, or (iii) are subject to additional cascading (sequential) or concomitant (simultaneous) hazards. Each of these cases implies a higher intra-event correlation, either on the input motion of the seismic event, the existence of additional follow-up seismic (e.g., aftershocks, tsunamis) and non-seismic events, or the propagation of the impact. Accounting for the latter requires a system-level model that can take care of cascading effects and interconnectivity (e.g., [2]). Furthermore, incorporating intra-event correlation of either hazard or damage requires some careful event-specific simulation, even in the “simple” case of a single seismic event or a cluster thereof [3, 4].

Within-event correlation for earthquakes is typically captured by employing event-based (or event-by-event) PSHA [5]. In contrast to the classical approach of Cornell [1], this is a Monte Carlo-based PSHA that relies on explicitly sampling a stochastic set of potential seismic events, from a seismic source model, each accompanied by one or more intensity measure (IM) fields that describe the event-specific spatial distribution of ground motion intensity. Follow-up or simultaneous events of seismic or non-seismic nature can be effectively tracked on this one-to-one basis, allowing comprehensive evaluation of damage accumulation and compounded consequences [6, 7]. Still, the norm in seismic assessments is to pair such event-by-event information with either class-generic or asset-specific fragilities. Essentially, we are disaggregating the seismic hazard into discrete events, while retaining the summarization of fragility/vulnerability functions. Still, record-to-record variability for a given IM value is non-negligible (e.g., [8–13]); even for single assets, it can range within 10%–40% or higher in terms of the coefficient of variation, depending on the structure, the level of response (pre-yield, post-yield, post-peak, etc.), and the IM itself. Crucially, this part of the dispersion in structural response pertains to the specific event: it is fully dependent on the waveform, that is, the shape of the ground motion record, since any IM dependence has been removed by the conditioning. One should expect that similar assets will behave similarly under and same recording at a given IM level, giving rise to the so-called waveform correlation. This disappears due to aggregation within a conventional fragility. How far such within-event correlated responses can influence the results of a seismic assessment, given such wide fragility dispersions, remains an open question. Fully answering it for the general case requires (i) some form of area-wide ground motion simulation, for example, physics-based simulation (e.g., [14]), which can generate correlated waveforms for sites within a geographical area for each specific event, as well as (ii) tracking the effect of said waveforms on each asset/system of interest. Eventually, this becomes a disaggregation of seismic hazard to discrete events and ground motions, as well as a disaggregation of conventional fragility/vulnerability curves, even to the extent

of removing the usefulness of the latter, as now structural analysis is required on an IM, record, and asset basis. Therefore, the resulting computational cost is indeed excessive, to the extent of infeasibility.

Still, there does exist a useful subset of seismic risk analyses where (i) event-by-event hazard analysis is not required and (ii) a physics-based simulation is not necessary; instead, near-perfect correlation of ground motion may need to be assumed to achieve fidelity. This is the typical case of collocated assets within an integrated facility of a relatively small footprint, such as a chemical plant, refinery, power plant, or similar (e.g., [15–18]). Then, for any event, the same IM level and the same ground motion, that is, a nearly identical waveform, is experienced by all assets of said facility. Depending on the degree of uniformity of soil conditions across the site, this similarity of IM and waveform may either hold at the soil surface or at the bedrock alone, in the latter case requiring at least some form of ground motion propagation to account for differing soil effects.

Given the prolific nature and importance of such cases, it becomes useful to offer a *per-record* approach that accounts for IM and waveform correlation by calculating event-specific, or rather seismic-record-specific, results. This is in contrast to the classic correlation-agnostic approach of the hazard curve and conventional seismic fragilities, which do not account for the correlation of asset structural responses within any given event. The straightforward way to retain the damage-to-ground-motion correlation in an interconnected system of multiple collocated assets (e.g., see [19–21]) is to avoid using fragilities altogether; instead, one can directly employ the results produced by each individual ground motion, evaluate the performance/integrity of the facility, and only then aggregate the results at the system level, that is, without taking any shortcut of intermediate aggregation across the different seismic records and assets considered.

Of course, considering correlation in damage to assets or components of a system in deriving the system probability of failure is certainly not new. For example, in the nuclear industry, it is the norm to account for common cause failures in power plant components and incorporate them in the overall probabilistic safety assessment [22, 23]. There are efficient algorithms in reliability theory, such as matrix-based approaches [24, 25], to incorporate asset correlations and propagate them to the system level. Still, these general approaches mostly cater to the efficient assessment of failure probabilities for complex systems. Instead, our focus is on quantifying and probabilistically characterizing the complex set of consequences at the system level, among others, allowing a direct consideration of cascading effects, direct/indirect monetary losses, socioeconomic impact, or business continuity, with full capabilities to slice and dice the results as one wishes [21].

To evaluate the difference between the two approaches, and thus the (suspected) bias of the conventional fragility approach in comparison to the more detailed per-record approach, different virtual systems/facilities are examined for both cases. Using 3D single-mass stick models of varying periods to represent different asset classes, three types of system topologies are examined: (i) single-class  $k$ -out-of- $n$  systems [26], that is, one asset class with  $n$  multiple identical members where at least  $k$  assets need to be functional to avoid failure, (ii) multi-class  $k$ -out-of- $n$  systems,

where the assets now come from multiple classes, and (iii) multi-class complex systems, where system-level failure is defined by a non-trivial fault tree [27–29]. For simplicity, assets belonging to a given class are assumed to be identical. This is characteristic of many facilities where multiple copies of a single asset type (e.g., a liquid storage tank, heat exchanger, pump, etc.) are present, although said “identical” assets may somewhat differ due to maintenance, content, quality of construction, etc.

For all assets, Incremental Dynamic Analysis (IDA [30]), is employed, using a set of hazard-consistent ground motion records (e.g., [31, 32]). Naturally, alternative methods, such as multi-stripe analysis [33] or cloud analysis [34, 35], can be similarly employed to the same effect. Apart from the personal preferences of one of the authors, we are making this choice for visual and comparative convenience, as it allows us to keep operating in terms of fragilities albeit on a record-by-record basis. Specifically, fragilities are calculated for each asset (or asset class) via two methods: (a) taking into account all ground motions per the conventional or *overall* fragility approach; (b) by calculating ground-motion-specific fragilities, according to the so-called per-record fragility approach (see [21]). In lieu of an actual impact assessment (e.g., in terms of direct/indirect losses), facility-level fragilities are calculated employing as a limiting threshold either a percentage of damaged assets (for  $k$ -out-of- $n$  systems), or the event of reaching a critical facility-level state (for systems with a fault tree). Overall, and within the limits of our assumptions, we expect the results to offer a useful test of whether, in what cases, and to what extent the consideration of ground motion waveform correlation (i.e., correlation of within-event characteristics beyond the IM value) can offer useful information for accurate seismic risk assessment.

## 2 | Alternative Fragility Approaches

### 2.1 | Fragility Definition

A high-level seismic performance study involves conducting multiple nonlinear response-history analyses under a suite of ground motion records. These analyses produce results that relate IMs, such as peak ground acceleration or spectral acceleration, to engineering demand parameters (EDP), such as drifts or forces. To exploit these IM-EDP datasets, so-called analytical fragility curves are typically employed to aggregate the calculated responses, linking the probability of exceeding a limit state (LS) to given IM values. The process of deriving these fragility curves is well-documented in the literature (e.g., [11, 36–39]). Their formal definition is:

$$F_{LS}(IM) = P[LS \text{ violated} | IM] = P[D > C_{LS} | IM] \quad (1)$$

where  $F_{LS}$  is the cumulative distribution function (CDF) of its argument,  $D$  is the EDP demand and  $C_{LS}$  is the EDP capacity threshold paired to a specific LS. When the EDP capacity threshold is exceeded, the corresponding LS is violated and the structure transitions into a higher damage state (DS). Adopting the typical lognormality assumption [40], fragility may be expressed as:

$$P[D > C_{LS} | IM] = \Phi\left(\frac{\ln IM - \ln IM_{LS50}}{\beta_{LS}}\right) \quad (2)$$

where  $IM_{LS50}$  is the median (50%) IM required to exceed LS, and  $\beta_{LS}$  is the lognormal dispersion. The latter may comprise only record-to-record variability, in IDA context estimated as the standard deviation of the natural logarithm of the set of IM values (one per ground motion employed) that results in LS violation. Further sources of uncertainty, for example, EDP capacity variability, may also be included. In our case, uncertainty in the capacity  $C_{LS}$  is considered and folded into  $\beta_{LS}$  via a simple Monte Carlo simulation, that is, by sampling multiple capacity values (following a lognormal distribution) when examining the exceedance of a DS, to properly capture this source of variability.

As a methodological remark, the “empirical CDF” fragility curves, that is, those derived by directly calculating the probability of LS exceedance at each IM level without applying any distribution model fitting, are employed hereinafter to ensure high fidelity in the results. They should not be confused with empirical fragilities, derived from observational data of actual earthquakes [41]. The fitted corresponding lognormal parameters, as per Equation (2), are only used for summarizing information in tables.

### 2.2 | Overall Versus Per-Record Fragilities

Fragility curves, as described in Section 2.1, group together the structural responses from all ground motion records considered. These are the conventional fragilities used in risk assessment studies and will hereafter be referred to as overall fragilities. The overall fragility approach is based on an aggregation scheme that inherently incorporates the aleatory uncertainty associated with the ground motion record-to-record variability. The critical point here is that the overall approach masks the distinct impact of individual ground motion characteristics (e.g., spectral content and pulse sequence) on a single structure, a portfolio of structures, or interconnected systems. In other words, it disconnects fragility estimates from the actual influence of the individual ground motion characteristics.

An alternative approach for evaluating the seismic performance of a structure in the framework of IDA relies on fragilities derived strictly from individual ground motion records, by examining the exceedance of the aforementioned EDP threshold, only accounting for the record at hand. Record-specific fragilities have already appeared in the literature, in the context of risk assessment for single assets (e.g., [9–11]). Still, they were only shown as an intermediate step to be eventually aggregated into overall fragilities and employed in a conventional manner. Contrarily, the per-record fragility concept espoused herein does not involve any such aggregation; instead, it retains the record-specific information throughout the seismic risk assessment path, preserving the effect of individual ground motion characteristics on asset response. Consequently, for a given asset, a set of fragilities (rather than a single one) can be produced per DS considered. Evidently, the number of fragility curves per DS equals the number of ground motion records that are employed in the analysis process. This set of fragilities characterizes each asset and will be referred to as per-record fragilities. A notable characteristic of the per-record fragility approach is that record-to-record variability is encoded in the set of record-specific fragilities, rather than any single one of them. In other words, the only dispersion appearing in individual

per-record fragilities is associated to other uncertainty sources (e.g., uncertainty in  $C_{LS}$ , model type, or model parameters) and can be incorporated, for example, via Monte Carlo simulation (e.g., [42]). For simplicity, only  $C_{LS}$  threshold-capacity variability will be considered as such an uncertainty source from this point onward. The following sections are devoted to further elucidating the aforementioned concepts and assessment workflow, complete with illustrative examples.

As a final remark, one can employ analysis approaches other than IDA to incorporate record-specific information. A prime example is multi-stripe analysis [33], whereby different ground motion records may be employed at different IM levels. Then, one cannot discuss record-specific fragilities, but instead should retain the results of each individual ground motion at each IM level. In the end, this is only a different bookkeeping exercise that can be naturally applied with multi-stripe results. On the other hand, the same cannot be claimed for cloud analysis [34, 35], at least not in its conventional form of modeling the IM-EDP relationship via a simple power law regression model [34]. An appropriate correlation model across all assets analyzed is necessary to ensure that the record-to-record linking is retained within the overall surrogate model that replaces individual record results in cloud analysis.

### 3 | Generic Assets and Fragilities

The two alternative approaches presented in Section 2 are comparatively studied using a set of simplified generic assets. These are modeled as single-mass linear oscillators with identical properties in the two principal axes, varying fundamental eigenperiods, and a damping ratio of 5%. Such simplified models are adopted for computational expediency, but also to offer a more transparent comparison of the results in fragility terms by expelling complexities that are often induced by actual structures, such as nonlinear behavior, plan and elevation irregularities, and higher mode effects. Ten structural typologies (or classes) of identical assets are employed, numbered I to X, reflecting ten different eigenperiods from 0.1 to 1.0 s with an increment of 0.1 s (Table 1).

The generic assets are located in a highly seismic region close to Athens, Greece. A set of 30 hazard-consistent ground motion records, each with two horizontal components of motion, is selected from the NGA-West2 database [43] using the conditional spectrum (CS) approach [31, 32] at a hazard level of 2% probability of exceedance in 50 years (see [18]). The selected ground motion records are natural non-pulse-like non-long-duration motions, and all analyses were performed by considering the horizontal excitation in both orthogonal directions. The records are numbered as R1 through R30. Full information about the selected set of ground motions is offered in an open-access repository [44]. The average spectral acceleration  $AvgSa(0.1 - 1.0s)$  is employed as the IM with a range of eigenperiods that encompass all the assets.  $AvgSa$  is calculated on the basis of the geometric mean of the two horizontal components of the employed ground motion records.

Note that we have avoided using simpler IMs, such as a spectral acceleration at a given period. Such a choice would not have played well with the use of elastic models for our study, as

**TABLE 1** | Asset class properties and lognormal fragility parameters, estimated for  $IM = AvgSa$ .

Asset Classes	Eigenperiod $T$ (s)	Median LS threshold $C_{LS50}$	Fragility parameters	
			$IM_{LS50}$ (g)	$\beta_{LS}$
I	0.10	0.001	1.38	0.58
II	0.20	0.005	1.27	0.54
III	0.30	0.010	1.15	0.45
IV	0.40	0.010	0.74	0.45
V	0.50	0.010	0.56	0.37
VI	0.60	0.020	0.88	0.32
VII	0.70	0.020	0.80	0.33
VIII	0.80	0.020	0.68	0.38
IX	0.90	0.030	0.90	0.40
X	1.00	0.030	0.83	0.43

it would zero out the record-to-record variability for elastic oscillators of matching periods, reduce it for nearby ones, and burden farther ones with considerably high dispersion. This could potentially bias our results. Instead, using  $AvgSa$  allows us to offer a moderately efficient IM for all elastic systems, without favoring any single one. In other words, via the adopted setup, all employed asset overall fragilities contain a healthy combination of record-to-record and capacity-threshold variability. Extensive studies employing more realistic nonlinear multi-degree-of-freedom models have reached similar conclusions [21], validating our approach.

A single damage state (DS) is defined for each generic asset, resulting in a binary structural condition, namely, either “no damage” (DS0) or “failure” (DS1). The asset’s maximum drift is adopted as the EDP, calculated via the maximum value of the square root of the sum of squares (SRSS) combination of the horizontal responses (in each timestep). Since drift and displacement response strongly depend upon the flexibility (or period) of the structure, different period-dependent capacity thresholds,  $C_{LS}$ , are assigned to each asset class. They are assumed to follow a lognormal distribution, with a 0.20 dispersion and a median value shown in Table 1. These medians are chosen to achieve roughly-similar-but-not-same probabilities of failure among the classes, largely ruling out a disproportionally strong influence from any single class. Instead, if a uniform median threshold was applied across all asset classes, short-period (stiff) structures would appear significantly less vulnerable, and the longest-period (flexible) ones would probably dominate the system performance, at least when considering drift values for defining fragility.

The overall empirical CDF fragilities are illustrated in Figure 1, and the corresponding lognormally fitted parameters (via the maximum likelihood estimation method, see [37]) are listed in Table 1. As mentioned earlier, the fitting is only performed for summarizing the fragilities in the table. All depictions and numerical usage of said fragilities employ the (superior) empirical CDF form. Note that one might expect the empirical CDF fragility of 30 records to look exactly like a staircase of 30 uneven steps.



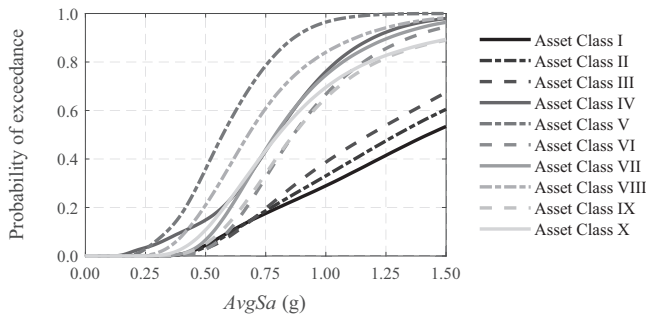


**FIGURE 1** | Asset classes' overall fragilities in their empirical CDF form.

This would indeed have been the case if there were no other sources of uncertainty. It is the consideration of the added uncertainty in  $C_{LS}$  that provides the smoothing effect seen in Figure 1. It may also be noted that despite the differing drift thresholds adopted, shorter period assets (I–III) are generally less vulnerable with median IM values of 1.2–1.4 g compared to the 0.7–0.9 g of moderate-period ones (VIII–X). The most vulnerable class is V at a period of  $T = 0.5$  s, having  $IM_{LS50} = 0.56$  g. Again, the target is not to have uniform fragility, only nearby levels thereof, mimicking actual portfolios. Finally, as mentioned earlier, despite using linear oscillators, the fragility dispersions are not unlike those of nonlinear systems, ranging between 0.32 and 0.58, of which the capacity threshold only contributes 0.2.

For comparison, the per-record fragilities for Classes III and VI are shown in Figure 2. Clearly, they provide a richer picture vis-à-vis the overall ones, demonstrating that single ground motions yield very different damage distributions. For instance, record R5 causes higher failure probabilities for asset Class III compared to R23, while for Class VI, R23 is more aggressive. This variability illustrates that per-record fragilities preserve the connection between specific ground motions and resulting damages, offering a more realistic depiction of their impact compared to overall fragilities.

#### 4 | System-Level Calculation Workflow

To evaluate how effectively the two approaches can manage systems of assets, different combinations of the generic asset classes shown in Table 1 are employed, for a total of  $m \geq 1$  assets in each case. For the purposes of our investigation, and in lieu of more complex impact metrics such as monetary losses, downtime, etc., the susceptibility of the system to earthquake-induced damage is assessed solely via a system-level fragility curve, indicating the probability of its failure given a specific IM level (IML). This probability curve is calculated via Monte Carlo Simulation. The calculation steps are presented as a Pseudo-algorithm in Figure 3.

For the overall fragility case,  $N$  realizations of the asset state are generated for each IML and asset by employing the corresponding fragility of Figure 1. Specifically, for every realization, a single DS is sampled per asset, depending on the corresponding failure probability (or probability of reaching a DS) of said asset given the IML. Hence, each asset is categorized as either undamaged (DS0) or failed (DS1). The calculation process is repeated for the entire

range of the considered IMLs. The same calculation procedure is applied in the case of the per-record fragility approach. The distinction lies in the sampling process: instead of drawing realizations from a single overall fragility function, sampling is carried out separately for each individual ground-motion record fragility. The resulting outcomes are then combined to derive the system fragility. To ensure a fair comparison with the overall fragility approach, the total number of realizations is kept consistent. Specifically, if  $N$  denotes the total number of realizations, each per-record fragility is assigned  $N/r$  realizations (where  $r$  is the number of ground-motion records), so that the aggregate number of realizations across all records remains equal to  $N$ .

Overall, the algorithm produces  $N$  realizations of the assets at each IML. In the overall fragility case, these realizations are record-agnostic, grouped together as they are randomly ordered by the Monte Carlo sampling, lacking any connection beyond corresponding to the same IML. For the per-record case, only asset realizations belonging to the same ground motion are considered together, by virtue of characterizing the same event. The occurrence of asset-specific failures is examined in each of the  $N$  realizations to check if the system-level failure criterion is met. This depends on the system-specific failure criteria defined in each case as discussed in the following Section 5.

#### 5 | System Case Studies

Interconnected systems may be spread over a wide area, for example, power transmission networks [45, 46], transportation networks [24, 47], gas distribution networks [48], or water supply systems [49]. Therein, due to the spatial variability in ground motion, an event-based rather than record-based disaggregation is more prudent. Other cases, though, are more geographically constrained and better fit within the per-record concept. Representative examples of such systems are nuclear power plants [50, 51], refineries [16, 19, 21] ports [52], and airports [53, 54]. Such are the case studies that will be targeted. To assess the differences between overall and per-record fragility approaches, the defined generic asset classes of Table 1 are used to evaluate alternative system topologies resembling realistic (but not real) cases. Said topologies differ in terms of the number and classes of assets involved, as well as the type of interconnection among them. The latter is effectively characterized by the adopted system failure criterion. Specifically, three system topologies are investigated.

The first topology involves systems of practically “identical” assets. These share the same structural characteristics and may be connected in series, in parallel, or partially-in-parallel [29]. Indicative actual cases of such systems are, for instance: small-scale tank farms comprising copies of the same liquid-storage-tank design, sign-supporting structures along a small segment of a highway, or telecommunication towers of a local cellular network. Despite being identical in design, such assets may still have differences, for example, due to aging, maintenance, operational modifications, or especially the filling level for liquid storage tanks [55, 56]. They are examined in Section 5.1 by considering a single asset class with a varying number of assets.

The second category includes more complex systems comprising diverse groups of “within-group-identical” assets. In other words,

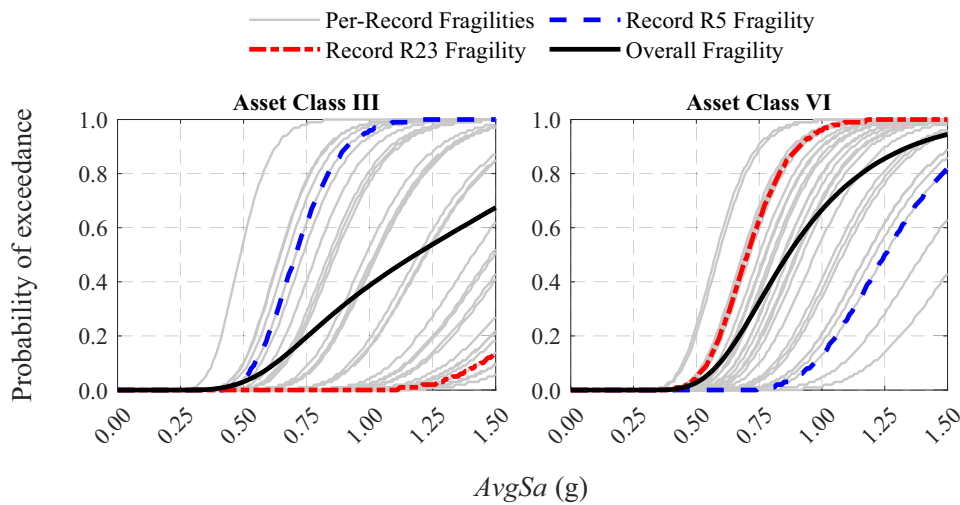


**FIGURE 2** | Overall fragility disaggregation to per-record fragilities for asset Classes III and VI. Indicatively, the fragilities obtained for specific records R5 and R23 [44] are highlighted with dash-dot (magenta) and dashed (blue) lines, respectively, against the solid (black) overall fragilities.

these are systems that contain structures of diverse characteristics, but often each type comes in multiple copies. They may also be connected in series, in parallel, or partially-in-parallel. Indicative real cases of such systems are for instance: tank farms involving different types of tanks (e.g., [21]), airports (control tower, terminals, hangars, fuel storage facility, auxiliary buildings, etc. [54]), and ports (docks, cranes, warehouses, etc. [52, 57]). This category is examined in Section 5.2 by considering systems with multiple asset classes with a varying number of assets per class.

Finally, critical systems with strongly interconnected assets are often associated with fault trees [27–29, 51, 58]. These systems involve components that are functionally dependent on one another, with those deemed critical having multiple redundancies. Thus, there are distinct failure paths that can lead to overall system disruption, where cascading events and common-cause failures become important considerations [59]. Typical examples are chemical processing plants [60], for example, crude-oil refineries and their distinct units [18–20], and nuclear power plants [61]. This category is examined in Section 5.3 by investigating simple fault trees to evaluate the performance of the system.

### 5.1 | Single-Class $k$ -out-of- $n$ Systems

The first category comprises systems where all assets come from the same class, essentially having the same structural properties and characterized by the same response under any given ground motion. Their only potential difference lies in the limit-state capacities/thresholds, which are taken herein as uncorrelated among the different systems. Thus, even within the per-record approach, there exists some variability in the damage of individual assets under the same ground motion due to capacity variability. Indicatively, only Class III assets are considered in the following format:

- a “system” comprising a single asset (1-asset system), as a benchmark;

- a system with three identical assets (3-asset system);
- a system with five identical assets (5-asset system);
- a system with ten identical assets (10-asset system).

Three system topologies are considered, namely: (i) a series system, where the system fails if at least one asset fails; (ii) a parallel system, where system failure is signaled by the simultaneous failure of all assets; and (iii) a partially-parallel system, where failure of a percentage of assets dooms the system. In reliability theory, all such topologies are collectively known as  $k$ -out-of- $n$  systems, where  $k$  assets out of  $n$  total need to be functional to avoid system failure. Thus,  $k = n$  corresponds to a classic series system,  $k = 1$  is the parallel one, while cases of  $1 < k < n$  are partially parallel/redundant ones. Note that such a system may be described in two equivalent ways: (i) the survival condition of “ $k$ -out-of- $n$  survive”, from where the naming convention is derived; (ii) the failure condition of “ $(n-k+1)$ -out-of- $n$  fail”. We will use the later version henceforth to characterize results, as it feels more natural.

System failure is examined by deriving the system-level curve (Section 4) using both the overall and the per-record fragility approaches. The results are illustrated for the series and parallel systems in Figure 4, indicating that the difference between the overall and per-record fragility approaches becomes more significant as the number of assets increases. The overall fragility approach tends to overestimate the failure probability for a series system, while it underestimates the failure probability for a parallel system. In other words, for such simple systems of two or more assets, the conventional approach is always biased.

To shed more light on the differences observed in Figure 4, the calculation of the system-level failure probability is presented for  $AvgSa = 1.0$  g for both approaches in a simpler format. At first, the failure probabilities of a single asset belonging to Class III are derived for each ground motion using the per-record fragilities; these are listed in Table 2. Averaging the per-record probabilities (as the records are considered equiprobable) results in the failure probability of the single asset as obtained from

## Pseudo-Algorithm: System-Level Fragility Assessment

### # Input:

Intensity Measure Levels:  $IML$   
 Number of Monte Carlo simulations:  $N$   
 Number of assets in system:  $m$   
 System failure criterion

### # System evaluation:

**For** the  $IML$  selected:

**If** the *Overall Fragility Approach* is employed:

Load the **overall fragilities** for each asset according to their asset class.

**For**  $i = 1$  to  $N$  realizations:

**For**  $j = 1$  to  $m$  assets:

Sample a **Damage State (DS)** based on the asset's fragility curve at current  $IML$

Assign state: **Failed (DS1)** or **Undamaged (DS0)**

**End**

Evaluate the **system-level failure** based on asset states and the system-specific failure criterion.

**End**

**End**

**If** the *Per-Record Fragility Approach* is employed:

Load the  $r$  **per-record fragilities** calculated separately for each ground motion record, for each asset according to their asset class.

**For**  $k = 1$  to  $r$  ground motion records:

**For**  $i = 1$  to  $N/r$  realizations:

**For**  $j = 1$  to  $m$  assets:

Sample a **Damage State (DS)** based on the asset's fragility curve at current  $IML$

Assign state: **Failed (DS1)** or **Undamaged (DS0)**

**End**

Evaluate the **system-level failure** based on asset states and the system-specific failure criterion.

**End**

**End**

**End**

For each  $IML$ , compute the fraction of simulations in which the system failed.

This gives the **system-level fragility** value at that  $IML$

**End**

### # Output:

System-level probability of failure per  $IML$ , as system-fragility curve, for the approach selected (overall or per-record)

**FIGURE 3** | Pseudo-algorithm for calculating the system-level fragility, indicating the probability of failure of the system for all  $IML$ s. The calculations can be performed for both the overall and per-record approach.

the overall fragility curve, that is, 38.7% (Figure 4). Rather than employing the (potentially obscure) Monte Carlo to derive the system-level failure probability, for the series and parallel system of (uncorrelated), assets this can be analytically computed for a given IM level as follows (e.g., [29]):

- Series system:

$$P_{\text{fail}} = 1 - P(\text{no asset fails})$$

$$= 1 - \prod_{i=1}^n P(\text{asset } i \text{ does not fail}) = 1 - (1 - p)^n \quad (3)$$

- Parallel system:

$$P_{\text{fail}} = \prod_{i=1}^n P(\text{asset } i \text{ fails}) = p^n \quad (4)$$

where  $n$  is the number of identical assets and  $p$  is the probability of failure of each individual asset. For the example at hand, if employing the overall fragility,  $p = 38.7\%$ , while if going the per-record way,  $p = 99\%$  for record R1,  $p = 1\%$  for record R2, and so on and so forth.

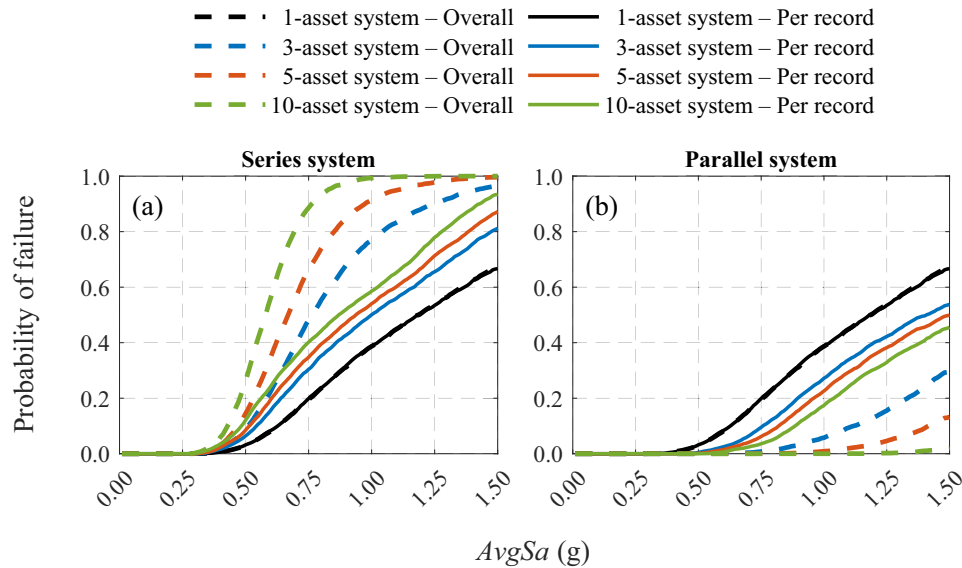


**FIGURE 4** | System-level probability of failure curves, by employing the overall and per-record approach, considering systems with varying numbers of identical Class III assets: (a) series system and (b) redundant system.

**TABLE 2** | Asset Class III: Per-record probabilities of single asset failure for  $AvgSa = 1.0$  g. Averaging the per-record probabilities yields the probability obtained from the overall fragility.

Record ID [44]	Per-record Probabilities	Record ID [44]	Per-record Probabilities
R1	0.99	R16	0.00
R2	0.01	R17	0.53
R3	0.00	R18	0.01
R4	1.00	R19	0.98
R5	0.96	R20	0.99
R6	0.77	R21	0.02
R7	0.16	R22	0.94
R8	0.04	R23	0.00
R9	0.00	R24	0.45
R10	0.47	R25	0.19
R11	0.79	R26	0.02
R12	0.00	R27	0.00
R13	0.16	R28	0.88
R14	0.00	R29	0.81
R15	0.44	R30	0.00
<b>Average probability</b>			0.387

Continuing with the overall fragility, for a 3-asset series system, Equation (3) yields a system-level probability of failure is equal to 77.0%. Accordingly, for the 5-asset series system, this increases to 91.3% due to the inclusion of more assets. Contrarily, in a parallel system, applying Equation (4) yields probabilities of 5.8% for the 3-asset system and 0.9% for the 5-asset system. As expected, failure of the parallel system is much rarer, and its probability is further lowered by the inclusion of more assets. Still, the usage of Equations (3) and (4) assumes no correlation, which we know

to be unrealistic for collocated assets. The per-record approach solves exactly this aspect.

For the per-record approach, Equations (3) and (4) are applied to each ground motion individually, and the results are then averaged across all records, as shown in Table 3. Now, benign and aggressive records make their presence evident across all assets; for the series system, the failure probabilities drop to 49.8% for the 3-asset system and 53.7% for the 5-asset system, much lower than the 77.0% and 91.3% estimates, respectively, of the overall fragility. Contrarily, the parallel systems receive higher failure probabilities at 27.3% and 23.0%, compared to the overall approach results of 5.8% and 0.9%, respectively. By showcasing the calculations step-by-step it becomes clear that these discrepancies only arise from the stage where record-aggregation occurs. When it is performed at an early stage, that is, before examining the effect of each record regarding the entire system, bias is inevitable, at least for such simple systems.

Partially parallel systems can be considered as intermediate cases, between series and parallel ones, and their behavior mirrors this. Indicatively, results are only shown for the 10-asset system under three failure conditions: (i) failure of at least 3-out-of-10 assets, (ii) failure of at least 5-out-of-10 assets, and (iii) failure of at least 7-out-of-10 assets simultaneously. The obtained system failure curves are compared in Figure 5. Contrarily to the series and parallel systems, the per-record fragility is not uniformly higher or lower vis-à-vis the overall one; instead, the two intersect, with the intersection point rising in IM as the number of assets needed to fail increases. In other words, the partially parallel system shows parallel-like behavior for low IMLs (or low probabilities) and series-like for high IMLs (or probabilities).

To better understand the results illustrated in Figure 5, let us dissect the underlying mechanism via a simplified version of case (ii) above. Consider a system of 10 *identical & deterministic* assets—that is, only record-to-record variability is considered, disregarding capacity uncertainty—subjected to 10



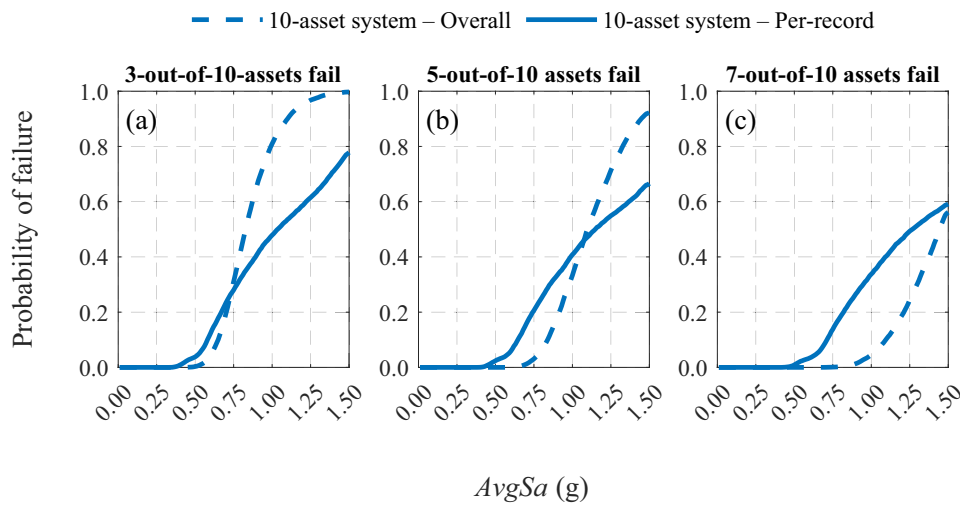


**FIGURE 5** | Comparison of system failure curves for the system of ten Class III assets by employing the overall and the per-record fragility approach: Simultaneously failure of at least (a) 3-out-of-10 assets, (b) 5-out-of-10 assets, and (c) 7-out-of-10 assets.

ground motion records, where failure is defined by 5-out-of-10 assets failing. Let us consider a (relatively low) IML, where the overall fragility yields a 30% asset failure probability. Then, using the overall fragility approach, each record would cause the failure of three assets on average, resulting to a  $\sim 0\%$  probability of system failure. Contrarily, when the per-record fragility approach is applied, the 30% overall probability is disaggregated exactly into three aggressive records, and seven benign ones. Then, the three aggressive records result in all (identical & deterministic) assets failing, while the remaining seven records cause no failures. In this case, the per-record approach yields a 30% system failure probability vis-à-vis the  $\sim 0\%$  outcome for the overall approach. Proceeding to a higher IML where the overall fragility yields 60% asset failure probability, the overall approach predicts 6 ( $>5$ ) failures on average, giving a  $\sim 100\%$  system failure probability. On the other hand, the per-record approach, disaggregates the 60% asset failure into six aggressive and four benign records. Again, the aggressive records cause failure of all assets, while the benign ones damage none. Thus, the per-record failure probability of the system is 60%, compared against the  $\sim 100\%$  result of the overall approach. In other words, we should always expect this crossing of fragilities appearing in Figure 5 wherever  $k$ -out-of- $n$  systems ( $1 < k < n$ ) are considered. Most importantly, for the critical low-IM region where the more frequent intensities appear, the overall approach will be universally unconservative.

## 5.2 | Multi-Class $k$ -out-of- $n$ Systems

This system topology is meant to investigate systems that comprise a variety of structural typologies. A  $k$ -out-of- $n$  failure criterion is adopted, considering the percentage of assets that have failed regardless of the class where they belong. This characterizes systems that rely on the collective functionality of their components rather than on the direct dependencies between them, making the percentage of damaged assets a critical factor for their performance. Examples of such systems may be port facilities, where cranes, warehouses, and docking areas operate independently, but if too many cranes or cargo handling systems fail, the overall port operations slow down or halt. Similarly,

cellular telecommunication networks depend on a distributed system of towers, where local failures are tolerable, but if a critical number of towers are damaged, coverage gaps emerge, leading to widespread communication disruptions. In all these systems, the spread of damage across their assets determines whether they continue to function (even at a reduced capacity) or fail.

The following systems are examined:

- a system with 10 asset Classes (I to X) and 1 asset in each class;
- a system with 10 asset Classes (I to X) and 3 assets in each class;
- a system with 10 asset Classes (I to X) and 5 assets in each class.

These systems utilize all previously defined asset classes (see Section 3) to capture a wide range of eigenperiods, reflecting the variability of assets within a typical system. Additionally, the systems are selected to examine the impact of having groups of identical assets within an otherwise diverse asset ensemble. The system-failure criterion is (indicatively) set to 10% or 20% of assets failing, regardless of class.

System-level curves were obtained for both approaches by employing the algorithm of Figure 3; they are illustrated in Figure 6. The key observation is that the results resemble those of single-class  $k$ -out-of- $n$  systems, but with significantly lower differences. Having different asset classes reduces the effect of record correlation introduced by the per-record approach. Actually, when a single asset is considered in each class, both fragility methods yield nearly identical results, as shown in Figure 6a. However, as the number of “identical” assets in each class increases, the correlation between the ground motions and the structural responses becomes more pronounced (Figures 6b,c), increasing the differences between the two approaches. The percentage of assets adopted as a system failure criterion does not seem to matter, at least not at the low percentages (10%–20%) employed.

Moving on to the investigation of more complex cases, four additional systems comprising all 10 classes are examined, each

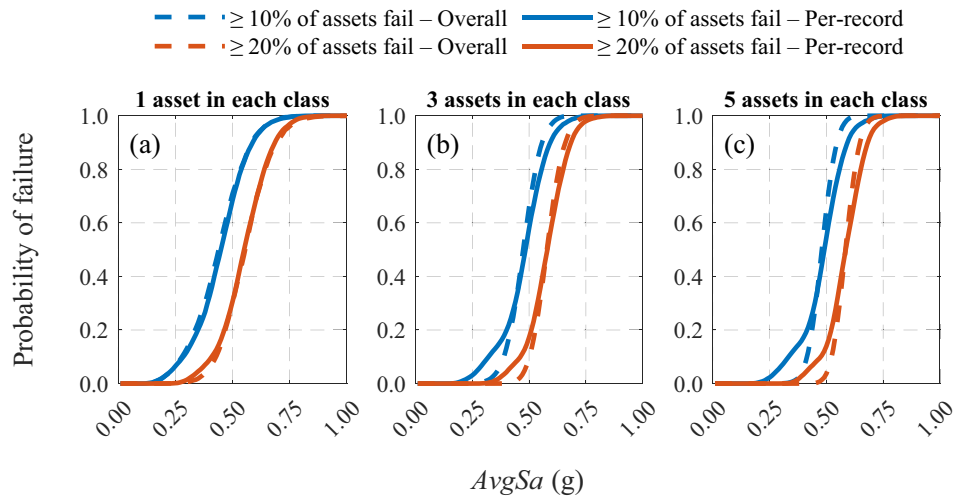


**FIGURE 6** | System fragility comparison for multi-class  $k$ -out-of- $n$  systems considering 10 asset classes with (a) 1 asset per class, (b) 3 assets per class, and (c) 5 assets per class.

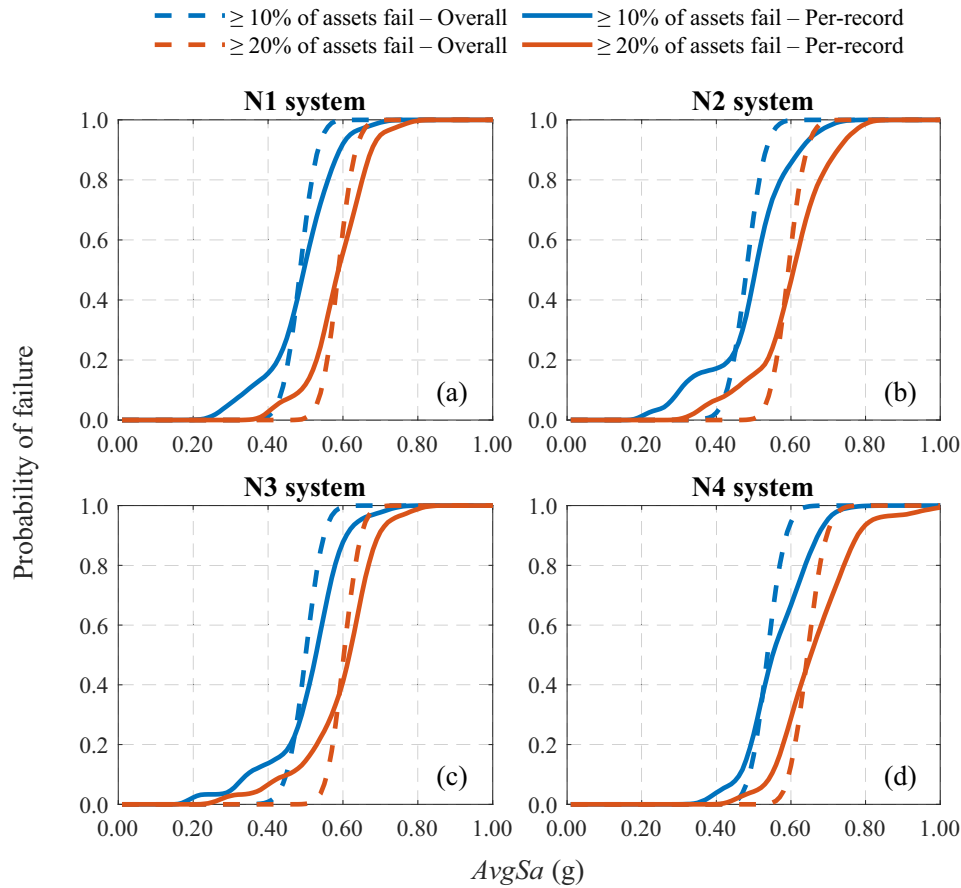


**FIGURE 7** | Comparison of system failure curves when following the overall or per-record approach considering multi-class systems N1 to N4 of 100 total assets (see Table 4) for 10% and 20% of assets failing.

having a total of 100 assets evenly or unevenly distributed among the classes (Table 4). In system N1, each class has the same number of assets, namely 10, while in systems N2 through N4, the number of assets in each class is uneven and arbitrarily chosen. The system failure probability curves are presented in Figure 7. By inspection, it is evident that the differences between the two employed fragility approaches are more profound compared to

the systems with fewer assets (see Figure 6). This verifies once more that these differences are affected by the number of assets in each class and the correlation of failures of identical assets. Another notable observation (see Figure 7) is that the bias of the conventional approach compared to the per-record can also be affected by the distributions of assets (systems N1–N4). As expected, when more assets come from the less vulnerable Classes

**TABLE 3** | Asset Class III: Per-record and system-level probabilities of failure for  $AvgSa = 1.0$  g, for the 3-asset and 5-asset series/parallel systems.

Record ID [44]	Series system <sup>a</sup>		Parallel system <sup>b</sup>	
	3 assets	5 assets	3 assets	5 assets
R1	1.000	1.000	0.970	0.951
R2	0.030	0.049	0.000	0.000
R3	0.000	0.000	0.000	0.000
R4	1.000	1.000	1.000	1.000
R5	1.000	1.000	0.885	0.815
R6	0.988	0.999	0.457	0.271
R7	0.407	0.582	0.004	0.000
R8	0.115	0.185	0.000	0.000
R9	0.000	0.000	0.000	0.000
R10	0.851	0.958	0.104	0.023
R11	0.991	1.000	0.493	0.308
R12	0.000	0.000	0.000	0.000
R13	0.407	0.582	0.004	0.000
R14	0.000	0.000	0.000	0.000
R15	0.824	0.945	0.085	0.016
R16	0.000	0.000	0.000	0.000
R17	0.896	0.977	0.149	0.042
R18	0.030	0.049	0.000	0.000
R19	1.000	1.000	0.941	0.904
R20	1.000	1.000	0.970	0.951
R21	0.059	0.096	0.000	0.000
R22	1.000	1.000	0.831	0.734
R23	0.000	0.000	0.000	0.000
R24	0.834	0.950	0.091	0.018
R25	0.469	0.651	0.007	0.000
R26	0.059	0.096	0.000	0.000
R27	0.000	0.000	0.000	0.000
R28	0.998	1.000	0.681	0.528
R29	0.993	1.000	0.531	0.349
R30	0.000	0.000	0.000	0.000
<b>Average probability</b>	0.498	0.537	0.273	0.230

<sup>a</sup>Calculated using Equation (3).<sup>b</sup>Calculated using Equation (4).

I–III, as in case N4, fewer overall assets govern the system failure, thus reducing the bias and vice-versa.

Instead of focusing on specific failure criteria, one could also evaluate how many assets will fail. This is typical of portfolio loss assessment, and it reflects the overall loss rather than any specific disruption metric. Figure 8 presents the percentage of failed assets in System N1 for each record and two indicative IMLs,  $AvgSa = 0.5$  g and 0.8 g. The overall approach is obvi-

**TABLE 4** | Alternative systems N1–N4 with 10 classes and different numbers of assets in each class.

Asset classes	Number of assets per class			
	N1	N2	N3	N4
I	10	15	5	15
II	10	10	10	10
III	10	20	5	30
IV	10	15	20	5
V	10	15	8	3
VI	10	10	20	2
VII	10	2	15	15
VIII	10	3	2	5
IX	10	5	10	10
X	10	5	5	5
Total number of assets	100	100	100	100

ously record-independent, providing an average failure estimate (shown as a flat line) around which the per-record results vary. Per the results of Figure 8, for  $AvgSa = 0.5$  g we can count 16 records with  $\geq 10\%$  failures, while the overall fragility yields slightly above 10% assets failing, obviously regardless of the record. Consequently, at  $AvgSa = 0.5$  g (Figure 8) system N1 displays a  $\sim 16/30 \approx 53\%$  failure probability or the per-record compared to 100% for the overall. Still, if one takes the average number of failed assets across all records, the same percentage of  $\sim 10\%$  is derived. In other words, when comparing the two approaches, the metric employed matters. When checking ensemble averages, the difference between the per-record and overall approaches practically disappears. This is confirmed by Figure 9, showing failure percentages across multiple IMLs. The overall and per-record approaches yield identical results, despite the deviations observed in individual record curves, indicatively shown for R5 and R23. This is good news for portfolio or regional loss assessment studies, where one is interested in metrics such as average annual loss, rather than the failure of a few critical assets. Both methods are effectively interchangeable in this context.

### 5.3 | Multi-Class Fault-Tree Systems

Fault tree systems and their analysis are standard practice in critical facilities, such as nuclear power plants, where system failure is determined by specific combinations of individual component failures (e.g., [27, 28, 51, 58]). Similar to Section 5.2, fault tree systems are multi-class, typically involving multiple components of different characteristics, but also redundant identical components. Interconnectivity usually appears in the form of having different components connected in series due to functionality (e.g., piping, pump, and its control panel), and then said series appearing in multiple redundant copies functioning in parallel to achieve enhanced levels of reliability. Two generic fault trees are defined herein (see Figure 10) to explore the effect of waveform correlation. Both systems have four different asset Classes (A, B, C, D), and employ OR/AND gates, with different

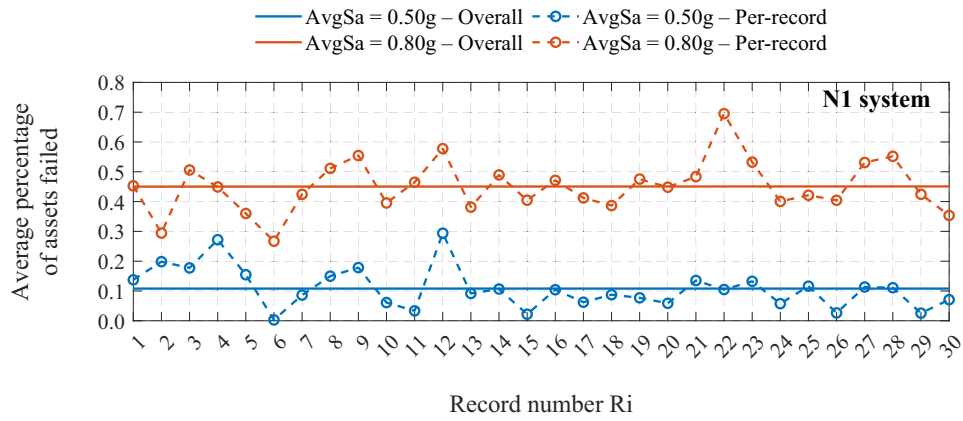


**FIGURE 8** | N1 system: Overall versus per-record fragility assessment results comparison for  $AvgSa = 0.5$  g and 0.80 g in terms of the average percentages of assets failing.

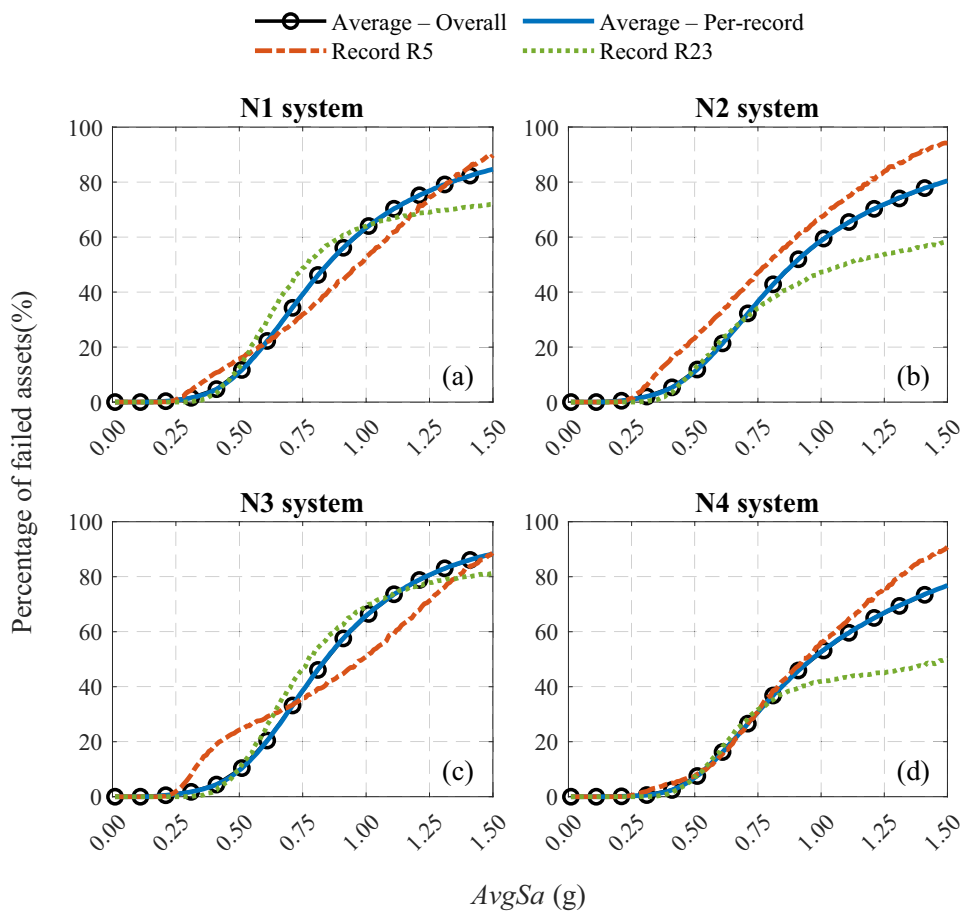


**FIGURE 9** | N1 system: Percentage of assets failed assessed using (i) the overall fragility approach results, (ii) the per-record approach, (iii) the ground-motion-specific R5 results, and (iv) the ground-motion-specific R23 results.

combinations in terms of which components must fail to reach system failure:

- Fault Tree #1 (FT1) represents a redundant system of series subsystems. Specifically, there are three series subsystems, each comprising four different components (A, B, C, and D). The failure of a single component in each subsystem signals its

failure. System failure requires the simultaneous failure of all three subsystems due to the triple redundancy. Equivalently, this translates to the failure of at least one component in each of the three subsystems. An example of such a topology is the top two levels of the loss-of-cooling-capacity fault tree for the *triple-redundant* diesel-generator subsystems of a nuclear power plant: All three generator subsystems need



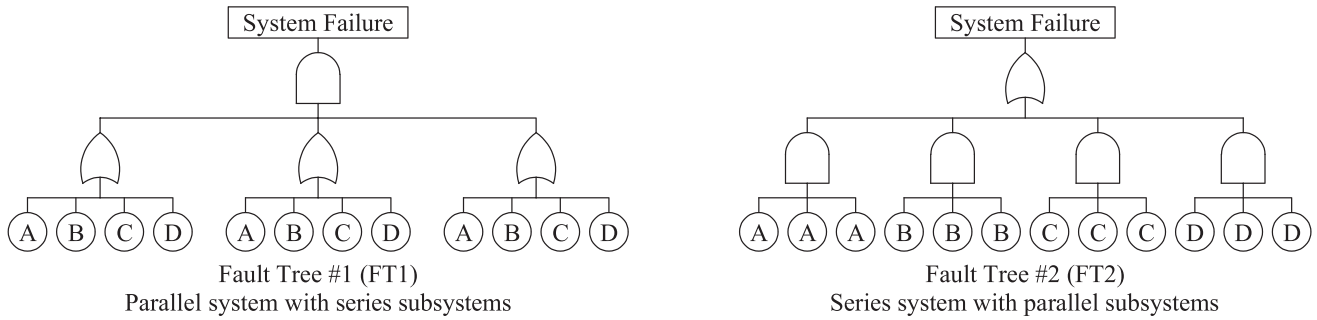
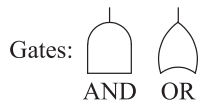


**FIGURE 10** | Fault trees considered in the investigation.

**TABLE 5** | Definition of multi-class fault tree systems S1–S4 in terms of fault tree topology (per Figure 10) and asset class considered for each component type (per Table 1).

Systems	Fault tree	Component A	Component B	Component C	Component D
S1	FT1	Asset Class III	Asset Class V	Asset Class VII	Asset Class VIII
S2	FT1	Asset Class I	Asset Class II	Asset Class IV	Asset Class VI
S3	FT2		Same as S1		
S4	FT2		Same as S2		

to fail to cause this emergency backup system to fail (e.g., see [62]).

- Fault Tree #2 (FT2) represents a series system of redundant subsystems. There are four such subsystems, each one comprising three identical components in parallel. Due to the triple redundancy within the subsystem, its failure is signaled by the simultaneous failure of all its components. System failure is triggered by the failure of at least one subsystem. A characteristic example of such a topology appears in process units of crude-oil refineries, where multiple pumps and heat exchangers are often present. The different equipment types operate in series, but there are at least two copies of each (master/spare) that function in parallel. This is for reasons of both periodic maintenance needs and operational safety to ensure that the process is not interrupted if a single piece of equipment is out of order; still, both component types are required to ensure continuous operation.

Based on the aforementioned fault tree topologies and considering alternative class make-ups of the underlying components, four systems are defined; they are denoted as S1 through S4, and their full details appear in Table 5. Clearly, the weaker component is B (Class V with  $IM_{LS50} = 0.56$  g) for S1/3 and C (Class IV with  $IM_{LS50} = 0.74$  g) for S2/4. We can expect that these will have a non-negligible role in the overall system performance.

The system-failure curves are calculated using both the overall and per-record fragility approaches by employing the calculation process of Section 4. The results are presented in Figure 11. The conventional approach (overall fragility) underestimates failure

probabilities at all IM levels, producing unconservative failure estimates. This is a direct consequence of having near-identical components involved in all redundancies. Systems S1/3 following FT1 topology will fail if all (weaker) components B fail at the same time; each subsystem contains at least one component B, which can single-handedly terminate its operation. This occurrence of simultaneous component B failures is smoothed over multiple records in the overall case, but appears more frequently for the per-record one due to accounting for waveform correlation. Similarly, the failure of all components C in systems S2/4 following FT2 topology will cause one of the series subsystems to stop operating, leading to system failure. The same thing can happen for any single type of components, exacerbating this trend.

While the considered examples are indicative, they clearly showcase that the inconsistencies observed between the two fragility approaches can lead to non-conservative system damage estimates, especially when complex systems are examined with combinations of series/redundant subsystems comprising multiple identical, similar, or essentially different components. Thus, the damage-to-ground-motion correlation remains relevant for such systems; ignoring it can lead to results of low fidelity for the system safety.

## 6 | Conclusions

Two alternative approaches for undertaking a seismic failure assessment in different kinds of interconnected systems have been examined to investigate their effect on seismic damage

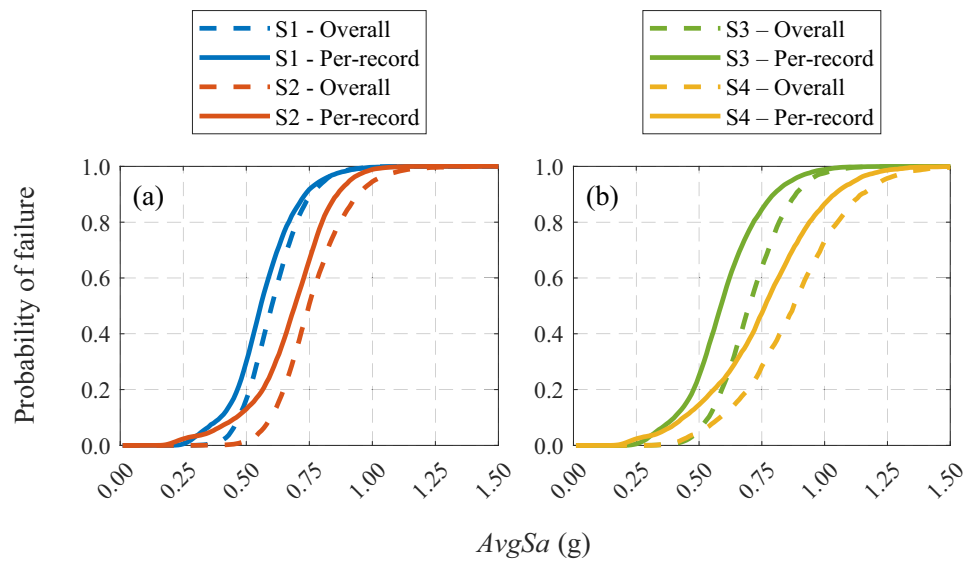


**FIGURE 11** | Comparison of system failure curves by following the overall and per-record fragility approaches for systems S1–S4 (Table 5).

estimates. The focus is on a critical interconnected system comprising a variety of structural typologies. Alternative system types regarding the level of diversity between the assets' properties, the number of assets, the failure checks employed, and the interconnectivity between assets (series, parallel,  $k$ -out-of- $n$ , and fault tree systems) have been examined to encompass a wide range of real-world representative examples. The most important outcomes of the present investigation are summarized below:

- Aggregating individual-record results at the fragility level (overall or conventional approach) versus tracking them separately (per-record approach) can potentially yield fundamentally different results.
- In cases where the metric of interest is an aggregate one (e.g., average loss), such differences are effectively smoothed over. Thus, the different approaches do not indicate a bias in terms of regional loss assessment case studies.
- On the contrary, when the metric of interest concerns a critical facility where failure of  $k$ -out-of- $n$  components or a certain combination of components leads to disruption, said differences are more pronounced.
- In cases where there is stronger damage-to-ground-motion correlation between assets, for example, due to having multiple near-identical assets, then the differences are stronger.
- The effect is asymmetric, sometimes generating conservative and sometimes unconservative bias depending on system topology, but also on the level of intensity (or probability of individual asset failure).

It should be noted that, for each system case, ground motion records were assumed to be applied uniformly to all assets, implying perfect correlation in both waveform and intensity. This simplification disregards potential spatial variability in seismicity or local soil conditions, which could alter ground motion characteristics at different locations. However, in this study, the assets are assumed to be located in relatively close proximity

(less than one kilometer apart), thus, the above assumption is deemed reasonable. For assets distributed over larger areas, this simplification may not hold, as spatial variability could significantly affect the results—although the fundamental advantages and limitations of the two approaches presented are not expected to change substantially.

In conclusion, the patterns observed in the different investigated system typologies reveal an underlying issue of the conventional fragility approach that cannot be ignored, since it is not clear *a priori* what is the extent of the induced bias in the system damage estimates due to the response aggregation. Thus, using the per-record approach or even in general a disaggregated, ground motion-specific evaluation of a critical system before any aggregation of results is performed, ensures that the ground motion-to-damage correlation patterns are still accounted for, leading to increased fidelity of the findings. This is especially crucial for risk assessment studies involving critical infrastructure, which highly rely on system damage estimates for developing their reactive and proactive seismic plans.

#### Acknowledgments

This research has been co-financed by the European Union through the HORIZON 2020 research and innovation programme “METIS–Seismic Risk Assessment for Nuclear Safety” under Grant Agreement No. 945121 and the HORIZON Europe innovation action “PLOT–Deployment and Assessment of Predictive modeling, environmentally sustainable and emerging digital technologies and tools for improving the resilience of IWW against Climate change and other extremes” under Grant Agreement No. 101069941.

The publication of this article in OA mode was financially supported by HEAL-Link.

#### Data Availability Statement

The data that support the findings of this study are available from the corresponding author upon reasonable request.

## References

1. C. A. Cornell, "Engineering Seismic Risk Analysis," *Bulletin of the Seismological Society of America* 58, no. 5 (1968): 1583–1606, <https://doi.org/10.1785/BSSA0580051583>.
2. L. Dueñas-Osorio, J. I. Craig, and B. J. Goodno, "Seismic Response of Critical Interdependent Networks," *Earthquake Engineering & Structural Dynamics* 36, no. 2 (2007): 285–306, <https://doi.org/10.1002/eqe.626>.
3. K. Goda and R. De Risi, "Multi-Hazard Loss Estimation for Shaking and Tsunami Using Stochastic Rupture Sources," *International Journal of Disaster Risk Reduction* 28 (2018): 539–554, <https://doi.org/10.1016/j.ijdrr.2018.01.002>.
4. A. N. Papadopoulos, P. Bazzurro, and W. Marzocchi, "Exploring Probabilistic Seismic Risk Assessment Accounting for Seismicity Clustering and Damage Accumulation: Part I. Hazard Analysis," *Earthquake Spectra* 37, no. 2 (2021): 803–826, <https://doi.org/10.1177/8755293020957338>.
5. R. M. W. Musson, "The Use of Monte Carlo Simulations for Seismic Hazard Assessment in the U.K.," *Annals of Geophysics* 43, no. 1 (2000), <https://doi.org/10.4401/ag-3617>.
6. K. Goda, "Nonlinear Response Potential of Mainshock–Aftershock Sequences From Japanese Earthquakes," *Bulletin of the Seismological Society of America* 102, no. 5 (2012): 2139–2156, <https://doi.org/10.1785/0120110329>.
7. A. N. Papadopoulos and P. Bazzurro, "Exploring Probabilistic Seismic Risk Assessment Accounting for Seismicity Clustering and Damage Accumulation: Part II. Risk Analysis," *Earthquake Spectra* 37, no. 1 (2021): 386–408, <https://doi.org/10.1177/8755293020938816>.
8. N. Shome, C. A. Cornell, P. Bazzurro, and J. E. Carballo, "Earthquakes, Records, and Nonlinear Responses," *Earthquake Spectra* 14, no. 3 (1998): 469–500, <https://doi.org/10.1193/1.1586011>.
9. C. Dymiotis, A. J. Kappos, and M. K. Chryssanthopoulos, "Seismic Reliability of RC Frames With Uncertain Drift and Member Capacity," *Journal of Structural Engineering (ASCE)* 125, no. 9 (1999): 1038–1047, [https://doi.org/10.1061/\(ASCE\)0733-9445\(1999\)125:9\(1038\)](https://doi.org/10.1061/(ASCE)0733-9445(1999)125:9(1038)).
10. A. K. Kazantzi, T. D. Righiniotis, and M. K. Chryssanthopoulos, "Fragility and Hazard Analysis of a Welded Steel Moment Resisting Frame," *Journal of Earthquake Engineering* 12, no. 4 (2008): 596–615, <https://doi.org/10.1080/13632460701512993>.
11. A. K. Kazantzi, T. D. Righiniotis, and M. K. Chryssanthopoulos, "A Simplified Fragility Methodology for Regular Steel MRFs," *Journal of Earthquake Engineering* 15, no. 3 (2011): 390–403, <https://doi.org/10.1080/13632469.2010.498559>.
12. M. Dolsek, "Incremental Dynamic Analysis With Consideration of Modeling Uncertainties," *Earthquake Engineering & Structural Dynamics* 38, no. 6 (2009): 805–825, <https://doi.org/10.1002/eqe.869>.
13. L. Ibarra and H. Krawinkler, "Variance of Collapse Capacity of SDOF Systems Under Earthquake Excitations," *Earthquake Engineering & Structural Dynamics* 40, no. 12 (2011): 1299–1314, <https://doi.org/10.1002/eqe.1089>.
14. R. Graves, T. H. Jordan, S. Callaghan, et al., "CyberShake: A Physics-Based Seismic Hazard Model for Southern California," *Pure and Applied Geophysics* 168 (2011): 367–381, <https://doi.org/10.1007/s00024-010-0161-6>.
15. S. Alessandri, A. C. Caputo, D. Corritore, R. Giannini, F. Paolacci, and H. N. Phan, "Probabilistic Risk Analysis of Process Plants Under Seismic Loading Based on Monte Carlo Simulations," *Journal of Loss Prevention in the Process Industries* 53 (2018): 136–148, <https://doi.org/10.1016/j.jlp.2017.12.013>.
16. A. C. Caputo, B. Kalemi, F. Paolacci, and D. Corritore, "Computing Resilience of Process Plants Under Na-Tech Events: Methodology and Application to Seismic Loading Scenarios," *Reliability Engineering and System Safety* 195 (2020): 106685, <https://doi.org/10.1016/j.ress.2019.106685>.
17. B. Kalemi, A. C. Caputo, D. Corritore, and F. Paolacci, "A Probabilistic Framework for the Estimation of Resilience of Process Plants Under Na-Tech Seismic Events," *Bulletin of Earthquake Engineering* 22, no. 1 (2024): 75–106, <https://doi.org/10.1007/s10518-023-01685-z>.
18. V. E. Melissianos, N. D. Karaferis, K. Bakalis, A. K. Kazantzi, and D. Vamvatsikos, "Hazard, Exposure, Fragility, and Damage state Homogenization of a Virtual Oil Refinery Testbed for Seismic Risk Assessment," *Earthquake Spectra* 41, no. 1 (2025): 547–578, <https://doi.org/10.1177/87552930241272521>.
19. C. Grajales-Ortiz, V. E. Melissianos, K. Bakalis, M. Kohrangi, P. Bazzurro, and D. Vamvatsikos, "Seismic Damage Assessment of a Crude Oil Hydrodesulphurisation Unit. Part I: Exposure and Modelling," *International Journal of Disaster Risk Reduction* 124 (2025):105519, <https://doi.org/10.1016/j.ijdrr.2025.105519>.
20. C. Grajales-Ortiz, V. E. Melissianos, K. Bakalis, M. Kohrangi, P. Bazzurro, and D. Vamvatsikos, "Seismic Damage Assessment of a Crude Oil Hydrodesulphurisation Unit. Part II: Hazard-Consistent Fragility Assessment," *International Journal of Disaster Risk Reduction* 124 (2025):105520, <https://doi.org/10.1016/j.ijdrr.2025.105520>.
21. N. D. Karaferis, V. E. Melissianos, K. Bakalis, A. K. Kazantzi, and D. Vamvatsikos, "Seismic Risk Assessment of a Crude Oil Refinery Testbed: Alternative Fragility Approaches," *International Journal of Disaster Risk Reduction* 124 (2025): 105495, <https://doi.org/10.1016/j.ijdrr.2025.105495>.
22. A. Mosleh, K. N. Fleming, G. W. Parry, H. M. Paula, D. H. Worledge, and D. M. Rasmuson, "Procedures for Treating Common Cause Failures in Safety and Reliability Studies: Analytical Background and techniques," *Nuclear Regulatory Commission, Washington, DC (USA). Div. Of Systems Research; Electric Power Research Inst. (EPRI) (Pickard, Lowe and Garrick, Inc., Newport Beach, CA, USA, 1988). (No. NUREG/CR-4780-Vol. 2; EPRI-NP-5613-Vol. 2; PLG-0547-Vol. 2).*
23. P. Hokstad and M. Rausand, "Common Cause Failure Modeling: Status and Trends," in *Handbook of Performability Engineering*, ed. K. B. Misra (London: Springer, 2008): 621–640, <https://doi.org/10.1007/978-1-84800-131-2>.
24. W. H. Kang, J. Song, and P. Gardoni, "Matrix-Based System Reliability Method and Applications to Bridge Networks," *Reliability Engineering & System Safety* 93 (2008): 1584–1593, <https://doi.org/10.1016/j.ress.2008.02.011>.
25. J. Song and W. H. Kang, "System Reliability and Sensitivity Under Statistical Dependence by Matrix-Based System Reliability Method," *Structural Safety* 31, no. 2 (2009): 148–156, <https://doi.org/10.1016/j.strusafe.2008.06.012>.
26. P. J. Boland and F. Proschan, "The Reliability of k out of n Systems," *Annals of Probability* 11, no. 3 (1983): 760–764, <https://www.jstor.org/stable/2243668>.
27. P.-C. ME, "Fault Trees vs. Event Trees in Reliability Analysis," *Risk Analysis* 4, no. 3 (1984): 177–186, <https://doi.org/10.1111/j.1539-6924.1984.tb00137.x>.
28. W. S. Lee, D. L. Grosh, F. A. Tillman, and C. H. Lie, "Fault Tree Analysis, Methods, and Applications—A Review," *IEEE Transactions on Reliability* R-34, no. 3 (1985): 194–203, <https://doi.org/10.1109/TR.1985.5222114>.
29. R. E. Melchers and A. T. Beck, *Structural Reliability Analysis and Prediction* (John Wiley & Sons, 2018), <https://doi.org/10.1002/9781119266105>.
30. D. Vamvatsikos and C. A. Cornell, "Incremental Dynamic Analysis," *Earthquake Engineering & Structural Dynamics* 31, no. 3 (2002): 491–514, <https://doi.org/10.1002/eqe.141>.
31. T. Lin, C. B. Haselton, and J. W. Baker, "Conditional Spectrum-Based Ground Motion Selection Part I: Hazard Consistency for Risk-Based Assessments," *Earthquake Engineering & Structural Dynamics* 42, no. 12 (2013): 1847–1865, <https://doi.org/10.1002/eqe.2301>.
32. M. Kohrangi, P. Bazzurro, D. Vamvatsikos, and A. Spillatura, "Conditional Spectrum-Based Ground Motion Record Selection Using Average Spectral Acceleration," *Earthquake Engineering & Structural Dynamics* 46, no. 10 (2017): 1667–1685, <https://doi.org/10.1002/eqe.2876>.



33. F. Jalayer and C. A. Cornell, "Alternative Non-Linear Demand Estimation Methods for Probability-Based Seismic Assessments," *Earthquake Engineering & Structural Dynamics* 38, no. 8 (2009): 951–972, <https://doi.org/10.1002/eqe.876>.
34. F. Jalayer, R. De Risi, and G. Manfredi, "Bayesian Cloud Analysis: Efficient Structural Fragility Assessment Using Linear Regression," *Bulletin of Earthquake Engineering* 13 (2015): 1183–1203, <https://doi.org/10.1007/s10518-014-9692-z>.
35. A. Miano, F. Jalayer, H. Ebrahimi, and A. Prota, "Cloud to IDA: Efficient Fragility Assessment With Limited Scaling," *Earthquake Engineering & Structural Dynamics* 47, no. 5 (2018): 1124–1147, <https://doi.org/10.1002/eqe.3009>.
36. V. Silva, H. Crowley, H. Varum, R. Pinho, and R. Sousa, "Evaluation of Analytical Methodologies Used to Derive Vulnerability Functions," *Earthquake Engineering & Structural Dynamics* 43, no. 2 (2014): 181–204, <https://doi.org/10.1002/eqe.2337>.
37. J. W. Baker, "Efficient Analytical Fragility Function Fitting Using Dynamic Structural Analysis," *Earthquake Spectra* 31, no. 1 (2015): 579–599, <https://doi.org/10.1193/021113EQS025M>.
38. K. Bakalis and D. Vamvatsikos, "Seismic Fragility Functions via Nonlinear Response History Analysis," *Journal of Structural Engineering (ASCE)* 144, no. 10 (2018): 04018181, [https://doi.org/10.1061/\(ASCE\)ST.1943-541X.0002141](https://doi.org/10.1061/(ASCE)ST.1943-541X.0002141).
39. V. Silva, S. Akkar, J. W. Baker, et al., "Current Challenges and Future Trends in Analytical Fragility and Vulnerability Modelling," *Earthquake Spectra* 35, no. 4 (2019): 1927–1952, <https://doi.org/10.1193/042418EQS101O>.
40. C. A. Cornell, F. Jalayer, R. O. Hamburger, and D. A. Foutch, "The Probabilistic Basis for the 2000 SAC/FEMA Steel Moment Frame Guidelines," *Journal of Structural Engineering (ASCE)* 128, no. 4 (2002): 526–533, [https://doi.org/10.1061/\(ASCE\)0733-9445\(2002\)128:4\(526\)](https://doi.org/10.1061/(ASCE)0733-9445(2002)128:4(526)).
41. T. Rossetto and A. Elnashai, "Derivation of Vulnerability Functions for European-Type RC Structures Based on Observational Data," *Engineering Structures* 25, no. 10 (2003): 1241–1263, [https://doi.org/10.1016/S0141-0296\(03\)00060-9](https://doi.org/10.1016/S0141-0296(03)00060-9).
42. A. K. Kazantzi, D. Vamvatsikos, and D. G. Lignos, "Seismic Performance of a Steel Moment-Resisting Frame Subject to Strength and Ductility Uncertainty," *Engineering Structures* 78 (2014): 69–77, <https://doi.org/10.1016/j.engstruct.2014.06.044>.
43. T. D. Ancheta, R. B. Darragh, J. P. Stewart, et al., "NGA-West2 Database," *Earthquake Spectra* 30, no. 3 (2014): 989–1005, <https://doi.org/10.1193/070913EQS197M>.
44. V. E. Melissianos, N. D. Kareferis, K. Bakalis, A. K. Kazantzi, and D. Vamvatsikos, "Exposure and Fragility of a Virtual Oil Refinery Testbed for Seismic Risk Assessment," *OpenAIRE Project* (2024), <https://zenodo.org/records/11419659>.
45. M. Shinozuka, X. Dong, T. C. Chen, and X. Jin, "Seismic Performance of Electric Transmission Network Under Component Failures," *Earthquake Engineering & Structural Dynamics* 36, no. 2 (2007): 227–244, <https://doi.org/10.1002/eqe.627>.
46. L. Chang and Z. Wu, "Performance and Reliability of Electrical Power Grids Under Cascading Failures," *International Journal of Electrical Power & Energy Systems* 33, no. 8 (2011): 1410–1419, <https://doi.org/10.1016/j.ijepes.2011.06.021>.
47. I. Kilanitis and A. Sextos, "Integrated Seismic Risk and Resilience Assessment of Roadway Networks in Earthquake Prone Areas," *Bulletin of Earthquake Engineering* 17 (2019): 181–210, <https://doi.org/10.1007/s10518-018-0457-y>.
48. S. Esposito, I. Iervolino, A. d'Onofrio, A. Santo, F. Cavalieri, and P. Franchin, "Simulation-based Seismic Risk Assessment of Gas Distribution Networks," *Computer-Aided Civil and Infrastructure Engineering* 30, no. 7 (2015): 508–523, <https://doi.org/10.1111/mice.12105>.
49. N. Romero, T. D. O'Rourke, L. K. Nozick, and C. A. Davis, "Seismic Hazards and Water Supply Performance," *Journal of Earthquake Engineering* 14, no. 7 (2010): 1022–1043, <https://doi.org/10.1080/13632460903527989>.
50. US Nuclear Regulatory Commission. *Reactor Safety Study: An Assessment of Accident Risks in US Commercial Nuclear Power Plants (Vol. 2)* (National Technical Information Service, 1975).
51. J. H. Purba, D. T. S. Tjahjani, and D. Deswandri. (2019), "The Implementation of Fault Tree Analysis Approaches in Nuclear Power Plant Probabilistic Safety Assessment," in *AIP Conference Proceedings* (AIP Publishing, 2019); 2180, 1, <https://doi.org/10.1063/1.5135519>.
52. D. Pachakis and A. S. Kiremidjian, "Estimation of Downtime-Related Revenue Losses in Seaports Following Scenario Earthquakes," *Earthquake Spectra* 20, no. 2 (2004): 427–449, <https://doi.org/10.1193/1.1705655>.
53. N. J. Ashford, S. Mumayiz, and P. H. Wright, *Airport Engineering: Planning, Design, and Development of 21st Century Airports* (John Wiley & Sons, 2011), <https://doi.org/10.1002/9780470950074>. ISBN 9780470950074.
54. S. Hanaoka, Y. Indo, T. Hirata, T. Todoroki, T. Aratani, and T. Osada, "Lessons and Challenges in Airport Operation During a Disaster: Case Studies on Iwate Hanamaki Airport, Yamagata Airport, and Fukushima Airport During the Great East Japan Earthquake," *Journal of the Japan Society of Civil Engineers* 1, no. 1 (2013): 286–297, [https://doi.org/10.2208/journalofjsce.1.1\\_286](https://doi.org/10.2208/journalofjsce.1.1_286).
55. N. D. Karaferis, V. E. Melissianos, and D. Vamvatsikos, "Mechanical Modeling, Seismic Fragility, and Correlation Issues for Groups of Spherical Pressure Vessels," *Acta Mechanica* 235, (2024): 1563–1582, <https://doi.org/10.1007/s00707-023-03670-8>.
56. S. Caprinuzzi and M. Dolšek, "Seismic Performance Assessment of Non-Code-Conforming and Code-Conforming Supporting Structures of Elevated Tanks Using Conventional and Risk-Based Decision Models," *Engineering Structures* 227 (2021): 111469, <https://doi.org/10.1016/j.engstruct.2020.111469>.
57. J. W. Böse, *Handbook of Terminal Planning* (Springer, 2011): 433, <https://doi.org/10.1007/978-3-030-39990-0>. (Second Edition). ISBN 9783030399924.
58. E. Ruijters and M. Stoelinga, "Fault Tree Analysis: A Survey of the state-of-the-Art in Modeling, Analysis and Tools," *Computer Science Review* 15–16 (2015): 29–62, <https://doi.org/10.1016/j.cosrev.2015.03.001>.
59. L. Duenas-Orsorio and S. M. Vemuru, "Cascading Failures in Complex Infrastructure Systems," *Structural Safety* 31, no. 2 (2009): 157–167, <https://doi.org/10.1016/j.strusafe.2008.06.007>.
60. G. J. Powers and F. C. Tompkins Jr, "Fault Tree Synthesis for Chemical Processes," *Journal American Institute of Chemical Engineers Journal* 20, no. 2 (1974): 376–387, <https://doi.org/10.1002/aic.690200226>.
61. American Nuclear Society and the Institute of Electrical and Electronic Engineers, *PRA Procedures. Guide: A Guide to the Performance of Probabilistic Risk Assessments for Nuclear Power Plants, NUREG/CR-2300, Vols. 1 and 2* (U.S. Nuclear Regulatory Commission, 1983).
62. A. Gerontati, N. Karaferis, N. Šipčić, D. Vamvatsikos, P. Bazzurro, and C. Droszcz, "A Minimalistic Computational Testbed for Evaluating Fragility Assessment, Record Selection, and Intensity Measure Optimality for Nuclear Powerplants," in *proceedings of: 27th International Conference on Structural Mechanics in Reactor Technology (SMiRT 27)*, Yokohama, Japan, 2024.